PHYSICAL REVIEW D **81,** 035003 (2010)

Dilepton signals in the inert doublet model

Ethan Dolle,[*] Xinyu Miao,[†] Shufang Su,[‡] and Brooks Thomas[§]

Department of Physics, University of Arizona, Tucson, Arizona 85721 USA

(Received 1 October 2009; published 3 February 2010)

The inert doublet model is one of the simplest and most versatile scenarios for physics beyond the standard model. In this work, we examine the prospects for detecting the additional fields of this model at the LHC in the dilepton channel. We investigate a wide variety of theoretically and phenomenologically motivated benchmark scenarios, and show that within regions of model parameter space in which the dark-matter candidate is relatively light (between 40 and 80 GeV) and the mass splitting between the neutral scalars is also roughly 40–80 GeV, a signal at the 3σ to 12σ significance level can be observed with 100 fb^{-1} of integrated luminosity. In addition, even if the mass splitting between the neutral scalars is larger than M_Z, a signal of more than 3σ can be observed as long as the mass of the dark-matter candidate is around 40 GeV.

DOI: 10.1103/PhysRevD.81.035003 PACS numbers: 14.80.−j, 12.60.Fr

I. INTRODUCTION

The inert doublet model [1] (IDM) is one of the simplest extensions of the standard model (SM), yet it is also one of the most versatile. This scenario, in which the usual SM fields are supplemented by a single scalar SU(2) doublet which does not contribute to electroweak-symmetry breaking (EWSB) and couples to the gauge-boson sector but not the fermion sector, has a wealth of potential phenomenological applications. Perhaps the most intriguing of these stems from the recent observation [2] that the fields of this additional scalar doublet can provide a positive contribution to the oblique T parameter [3] sufficient to render a SM Higgs mass of $m_h = 400$–600 GeV consistent with precision data [4]. A host of other potential applications for inert[1] doublets exist as well. These range from explaining the lightness of neutrino masses via a one-loop radiative seesaw mechanism [5] to the loop-level induction of electroweak-symmetry breaking [6] to engineering successful grand unification [7]. Furthermore, the model yields a natural dark-matter candidate in the form of the lightest inert particle (LIP), whose absolute stability is guaranteed by an unbroken $\mathbb{Z}_2$ symmetry. Studies of the relic abundance of LIP dark matter [8,9], as well as its prospects for indirect detection via neutrino [10,11], cosmic-ray positron and antiproton [12], and gamma-ray [13,14] signatures, and for direct detection [15,16] have also been performed. An extension of this scenario in which right-handed neutrinos contribute significantly to the dark-matter relic density has also been proposed [17].

Since the coupling structure of the fields of the additional scalar doublet in the IDM differs from that of typical two-Higgs doublet models (2HDM) in the manner discussed above, the collider phenomenology of the IDM also differs markedly from that of such 2HDM. It is therefore worthwhile to investigate the prospects for detecting the additional fields of the IDM via their decay signatures at the Large Hadron Collider (LHC). In this work, we focus on the dilepton (plus missing energy) channel, which turns out to be one of the most auspicious channels in terms of its discovery potential. Some preliminary, parton-level studies of this channel have been conducted [18] within one particular region of parameter space. Here, we present a more comprehensive, detector-level analysis in which we investigate a variety of different benchmark regions motivated by dark-matter studies, etc., and assess the prospects for observing a $\ell^+\ell^- + \not{E}_T$ signal at the LHC in each regime. We note that the results of this analysis, although conducted in the context of the IDM, should also be applicable to other extensions of the SM with similarly modified scalar sectors, as long as the extra scalars in those extensions have similar decay patterns to those in the IDM.

We begin in Sec. II with a recapitulation of the inert doublet model. In Sec. III, we summarize the theoretical and experimental constraints to which the model is subject. We outline a set of representative benchmark points which correspond to phenomenologically interesting regions of the parameter space in which all of these constraints are satisfied. In Sec. IV, we discuss dilepton production in the IDM, as well as the SM backgrounds for $\ell^+\ell^- + \not{E}_T$ at the LHC, and we outline the event-selection criteria we use to differentiate signal events from those produced by these backgrounds. We present our numerical results in Sec. V, and in Sec. VI, we conclude.

[*]edolle@physics.arizona.edu
[†]miao@physics.arizona.edu
[‡]shufang@physics.arizona.edu
[§]brooks@physics.arizona.edu

[1]The descriptor ''inert'' is applied to the additional scalar doublet in the IDM in order to indicate that it does not couple to the SM fermions. We will therefore continue to refer to the fields this doublet comprises as inert particles, even though these particles are not truly inert in the sense that they have SM gauge interactions.

II. MODEL FRAMEWORK

The inert doublet model is an extension of the SM in which the Higgs sector comprises two scalar SU(2) doublets. The first of these doublets, here denoted ϕ_1, resembles the SM Higgs doublet $H_{\rm SM}$. It bears full responsibility for electroweak-symmetry breaking and its neutral component acquires a vacuum expectation value equal to that of the SM Higgs: $\langle \phi_1^0 \rangle = v/\sqrt{2} = 174$ GeV. It also couples to quarks and leptons in precisely the way $H_{\rm SM}$ does in the SM. The second doublet, here denoted ϕ_2, does not contribute to EWSB ($\langle \phi_2 \rangle = 0$), nor does it have Yukawa interactions with the SM quarks and leptons. This coupling structure is enforced by a $\mathbb{Z}_2$ symmetry under which

$$\phi_1 \to \phi_1, \qquad \phi_2 \to -\phi_2, \tag{1}$$

and all the SM fields transform trivially. This symmetry, sometimes called matter parity, remains unbroken in the vacuum, since $\langle \phi_2 \rangle = 0$. The most general CP-even scalar potential allowed by this $\mathbb{Z}_2$ symmetry is

$$\begin{aligned} V = {} & \mu_1^2|\phi_1|^2 + \mu_2^2|\phi_2|^2 + \lambda_1|\phi_1|^4 + \lambda_2|\phi_2|^4 \\ & + \lambda_3|\phi_1|^2|\phi_2|^2 + \lambda_4|\phi_1^\dagger \phi_2|^2 \\ & + \left[\frac{\lambda_5}{2}(\phi_1^\dagger \phi_2)^2 + \text{H.c.}\right]. \end{aligned} \tag{2}$$

After EWSB is triggered by the vacuum expectation value of ϕ_1, the scalar spectrum of the model comprises the usual SM Higgs h (the neutral, CP-even degree of freedom in ϕ_1), as well as four additional fields corresponding to the 4 degrees of freedom in ϕ_2. These include a pair of charged scalars $H^\pm$, a neutral, CP-even scalar S, and a neutral, CP-odd scalar A. The masses of these scalars, given in terms of the six free parameters[2] $\{\mu_2^2, \lambda_1, \lambda_2, \lambda_3, \lambda_4, \lambda_5\}$ in Eq. (2), are

$$m_h^2 = 2\lambda_1 v^2, \tag{3}$$

$$m_{H^\pm}^2 = \mu_2^2 + \lambda_3 v^2/2, \tag{4}$$

$$m_S^2 = \mu_2^2 + (\lambda_3 + \lambda_4 + \lambda_5)v^2/2, \tag{5}$$

$$m_A^2 = \mu_2^2 + (\lambda_3 + \lambda_4 - \lambda_5)v^2/2. \tag{6}$$

For our purposes, it will be useful to parametrize the model using the alternative parameter set $\{m_h, m_S, \delta_1, \delta_2, \lambda_2, \lambda_L\}$, where $\delta_1 \equiv m_{H^\pm} - m_S$, $\delta_2 \equiv m_A - m_S$, and $\lambda_L \equiv \lambda_3 + \lambda_4 + \lambda_5$. This parameterization is particularly useful in that it characterizes the model in terms of physically significant quantities such as particle masses, mass splittings, and λ_L: the coefficient which controls the trilinear hSS and quartic $hhSS$ couplings.

[2]The seventh parameter μ_1^2 appearing in Eq. (2) is fixed by the constraint $v^2 = -\mu_1^2/\lambda_1$ from EWSB.

The assumption of an unbroken $\mathbb{Z}_2$ matter parity renders at least one of the degrees of freedom in ϕ_2 absolutely stable. If this particle is electrically neutral (S or A in the IDM), it becomes a good weakly interacting-massive-particle dark-matter candidate. For the remainder of this work, we will assume that the LIP is the CP-even scalar S, and hence $\delta_2 > 0$. The phenomenology of the alternative scenario, in which the CP-odd scalar A plays the role of the LIP, is very similar.

III. MODEL CONSTRAINTS

A variety of considerations, stemming both from theoretical consistency conditions and from experimental bounds, constrain the IDM. Below, we briefly summarize these constraints, which were discussed in detail in Ref. [9].

(i) *Perturbativity*:

$$\lambda_3^2 + (\lambda_3 + \lambda_4)^2 + \lambda_5^2 < 12\lambda_1^2, \qquad \lambda_2 < 1. \tag{7}$$

(ii) *Vacuum stability*:

$$\begin{aligned} &\lambda_1 > 0, \qquad \lambda_2 > 0, \qquad \lambda_3 > -2\sqrt{\lambda_1 \lambda_2}, \\ &\lambda_3 + \lambda_4 - |\lambda_5| > -2\sqrt{\lambda_1 \lambda_2}. \end{aligned} \tag{8}$$

(iii) *Limits from direct collider searches*: First of all, the excellent agreement between the experimentally measured values for Γ_W and Γ_Z obtained from LEP and Tevatron data [19] and the predictions of the SM requires that

$$\begin{aligned} &2m_S + \delta_1 > M_W, \qquad 2m_S + \delta_1 + \delta_2 > M_W, \\ &2m_S + \delta_2 > M_Z, \qquad 2m_S + 2\delta_1 > M_Z, \end{aligned} \tag{9}$$

in order that the decays $W^\pm \to SH^\pm, AH^\pm$ and $Z \to SA$, H^+H^- are kinematically forbidden.

Second of all, bounds on the invisible decays of the Higgs boson from LEP data [20] also serve to constrain scenarios in which the Higgs is light and $m_h > 2m_S$. In this work, however, we will be primarily concerned with cases in which $m_h > 114$ GeV, for which the bounds from the searches on invisible Higgs decay does not apply.

Third and finally, one can consider limits arising from direct searches for $H^\pm$, A, and S, both at LEP and at the Tevatron [21,22]. It should first be noted that the standard limits on additional charged and neutral Higgs scalars do not apply, because the standard search channels from which they are derived generally involve the couplings of such scalars to fermions, which are absent in the IDM. On the other hand, bounds derived from the nonobservation of $e^+e^- \to \chi_1^0\chi_2^0$ [23] and $e^+e^- \to \chi_1^+\chi_1^-$ [24] decays in supersymmetric models can be used to constrain

the IDM parameter space, since $e^+e^- \to SA$ and $e^+e^- \to H^+H^-$ in the IDM lead to similar signals. A detailed analysis of the constraints on $e^+e^- \to SA$ in the IDM based on LEP II searches for $e^+e^- \to \chi_1^0\chi_2^0$ was conducted in Ref. [25], which showed that regions of parameter space with $m_S \lesssim 80$ GeV and $m_A \lesssim 100$ GeV for $\delta_2 \gtrsim 8$ GeV had been ruled out. For $\delta_2 \lesssim 8$ GeV, however, only the LEP I constraint $m_S + m_A > M_Z$ applies. A rough bound of $m_{H^\pm} \gtrsim$ 70–90 GeV [26] can also be derived from the LEP $e^+e^- \to \chi_1^+\chi_1^-$ limit by making the necessary modifications to account for the difference in cross section between fermion-pair and scalar-pair production. Taking these considerations into account, we will henceforth restrict our attention to models for which $m_{H^\pm} > 80$ GeV.

(iv) *Electroweak precision constraints*: Electroweak precision measurements set limits on contributions from the additional Higgs doublet to the oblique S and T parameters [3]. We consider a given parameter choice to be consistent with electroweak precision constraints as long as the overall values of S and T it yields, once all contributions are taken into account, lie within the 68% C.L. ellipse determined by the LEP Electroweak Working Group [27]. For a light SM Higgs, with $m_h \lesssim 200$ GeV, the constraint is weak as long as δ_1 and δ_2 are of roughly the same order. For a heavy SM Higgs, a large splitting between $H^\pm$ and S is preferred, and $\delta_1 > \delta_2$.

(v) *Dark-matter relic density*: One of the attractive aspects of the inert doublet model is that it can provide a viable weakly interacting-massive-particle dark-matter candidate in the form of a stable, neutral LIP. The model is therefore constrained by experimental limits on the relic density of dark matter in the Universe. In what follows, we will assume that the LIP relic density represents the dominant component of $\Omega_{\rm DM}h^2$ and falls within the 3σ range of the dark-matter density of the universe as measured by WMAP [28][3]: $0.085 < \Omega_{\rm DM}h^2 < 0.139$. A detailed examination of the relic density of a CP-even scalar LIP in the IDM was conducted in [9]. It was found that the correct dark-matter relic density could be realized in several distinct regions of parameter space in which all the aforementioned theoretical and experimental constraints were also satisfied. For a light SM Higgs with $m_h \sim 120$ GeV, two scenarios are possible. The first of these involves a light LIP with $m_S \sim 40$–80 GeV and mass splittings δ_1 and δ_2 which are sizeable, but of the same order. The second involves a heavier dark-matter particle with $m_S \gtrsim 400$ GeV and relatively small mass splittings. For a heavy SM Higgs with $m_h \gtrsim 400$ GeV, the regions which the constraints leave open are those in which $m_S \sim 80$ GeV and $\delta_1 > \delta_2$, with both δ_1 and δ_2 relatively large, or $m_S \sim$ 50–75 GeV, $\delta_2 \lesssim 8$ GeV with a large δ_1.

In Table I, we define a set of benchmark points, each designed to represent a particular region of the remaining, ''habitable'' parameter space, with an eye toward its collider phenomenology. We emphasize that each benchmark point in Table I is consistent with all of the applicable constraints detailed above, and that each yields an LIP relic density that falls within the WMAP 3σ range for $\Omega_{\rm DM}h^2$.

The first regime of interest involves a light SM Higgs with $m_h < 200$ GeV. For such Higgs masses, as discussed above, the electroweak precision constraints are not terribly stringent, and a wide variety of possible particle spectra are permissible. We have included five different benchmark points in our analysis which correspond to this regime (labeled LH1–LH5 for ''light Higgs''), the properties of which are listed in Table I. These points are representative of the set of possible scenarios which differ qualitatively from the perspective of a dilepton-channel analysis at the LHC. The points LH1 and LH2 both represent cases in which the LIP is light (~ 40 GeV) and δ_1 and δ_2 are large and of the same order. However, for the point LH1, $\delta_1 > M_W$ and $\delta_2 > M_Z$, meaning that both $H^\pm$ and A can decay on shell (to $SW^\pm$ and SZ, respectively), whereas for LH2, $\delta_1 < M_W$ and $\delta_2 < M_Z$, so only three-body decays are kinematically accessible. A slightly larger Higgs mass $m_h = 150$ GeV is mandated in LH1 by perturbativity constraints. However, the collider phenomenology of S, A, and, $H^\pm$—at least as far as the dilepton channel is concerned—does not depend significantly on the value of m_h, as will soon be made apparent.

Points LH3–LH5 all correspond to situations in which $m_S \sim 80$ GeV, but each represents a different relationship between δ_1 and δ_2. The point LH3 represents a situation

TABLE I. A list of benchmark points used in our analysis, defined in terms of the model parameters $\{m_h, m_S, \delta_1, \delta_2, \lambda_L\}$. Dark-matter relic density and collider phenomenology of the IDM depend little on λ_2, which is set to 0.1 for all benchmark points. The points LH1–LH5 involve a light (120 GeV $\leq m_h \leq$ 150 GeV) Higgs boson, while the points HH1–HH3 involve a heavy ($m_h = 500$ GeV) Higgs.

Benchmark	m_h (GeV)	m_S (GeV)	δ_1 (GeV)	δ_2 (GeV)	λ_L
LH1	150	40	100	100	−0.275
LH2	120	40	70	70	−0.15
LH3	120	82	50	50	−0.20
LH4	120	73	10	50	0.0
LH5	120	79	50	10	−0.18
HH1	500	76	250	100	0.0
HH2	500	76	225	70	0.0
HH3	500	76	200	30	0.0

[3]In the event that additional sources contribute to $\Omega_{\rm DM}h^2$, only the upper bound applies.

similar to that embodied by LH2, in which δ_1 and δ_2 are on the same order and on-shell decays to SA and $SW^{\pm}$ are inaccessible. Larger values of $\delta_{1,2} > M_{W,Z}$ are disfavored by the aforementioned battery of constraints. The point LH4 represent the case of intermediate δ_2 and small δ_1, while the point LH5 represents the opposite situation, in which δ_1 is of intermediate size and δ_2 is small. It is also possible to realize a situation similar to that of LH4, but with $\delta_2 > M_Z$ and hence on-shell A decay. The dilepton-channel analysis in this case would be similar to that in LH1 and HH1. Another possibility would be a point similar to LH5, but with $\delta_1 > M_W$, so that on-shell $H^{\pm}$ decays would be allowed. However, as will be explained in more detail below, the dilepton-signal contribution from H^+H^- decay is hard to disentangle from the SM W^+W^- background. Consequently, varying δ_1 has little effect on the observability of the dilepton signal via SA associated production, by far the most useful production process for discovery at the LHC.

The second regime of interest involves a heavy SM Higgs with $m_h \gtrsim 400$ GeV. A large splitting between $H^{\pm}$ and S is required to satisfy the constraints from electroweak precision measurements in this case. Broadly speaking, these constraints, taken in tandem with relic-abundance considerations, prefer δ_1 to be quite large (and generally much larger than δ_2) and the LIP mass to lie within the range $m_S \approx 70$–80 GeV [9]. This parameter-space regime is represented by the benchmark points HH1–HH3 (where ''HH'' stands for ''Heavy Higgs'') in Table I. The point labeled HH1 represents the case in which $\delta_2 > M_Z$ and A decays proceed via an on-shell Z intermediary, while the point HH2 represents the case in which $\delta_2 < M_Z$, and the decay $A \to SZ$ is kinematically inaccessible. HH3 is similar to HH2, but has a small $\delta_2 = 30$ GeV. Since precision constraints generally dictate that $m_H^{\pm} > m_A > m_S$ if S is to be the LIP, these three cases encapsulate the only qualitatively different possibilities in this regime from the perspective of dilepton-channel analysis. It is worth noting that another region of parameter space does exist in which all the aforementioned constraints are satisfied: one in which $50\ \text{GeV} \lesssim m_S \lesssim 75\ \text{GeV}$ and the mass splitting δ_2 is very small ($\delta_2 \lesssim 8$ GeV). However, a dilepton signal tends to be exceedingly difficult to observe in scenarios of this sort, due to the softness of the jets and leptons in the final states. For this reason, we do not include a representative benchmark point for this region in the present study.

For the other allowed region of parameter space—that in which $m_S \gtrsim 400$ GeV and the mass splittings δ_1 and δ_2 are relatively small—no benchmark points have been included in this study. This is because a scenario of this sort does not yield a detectable signal in the dilepton channel. One reason for this is that the pair-production cross sections for the inert scalars are highly suppressed due to their heavy masses. Another is that the jets and leptons produced during $H^{\pm}$ and A decays will be quite soft, owing to the small mass splittings $\delta_{1,2} \lesssim 2$ GeV required in such scenarios in order to reproduce the WMAP relic density [9]. Therefore, although it remains a phenomenologically viable scenario, we will not discuss this possibility further in the present work.

IV. SIGNALS, BACKGROUNDS, AND EVENT SELECTION

Let us now turn to examine the signal and background processes relevant to an analysis of the dilepton channel in the IDM at the LHC. The inert scalars $H^{\pm}$, A, and S can be pair produced directly at the LHC by Drell-Yan processes involving virtual photons and $W^{\pm}$, Z bosons:

$$\begin{aligned} &q\bar{q} \to Z \to AS, \qquad q\bar{q} \to Z/\gamma^* \to H^+H^-, \\ &q\bar{q}' \to W^{\pm} \to AH^{\pm}, \qquad q\bar{q}' \to W^{\pm} \to SH^{\pm}. \end{aligned} \tag{10}$$

In Table II, we listed the production cross sections for SA, H^+H^-, $SH^{\pm}$, and $AH^{\pm}$ at the LHC for the various benchmark points defined in Table I. Once so produced, the unstable $H^{\pm}$ and A bosons further decay to lighter states plus $W^{(*)}$ or $Z^{(*)}$. Depending on how $H^{\pm}$ and A decay, a number of final states are possible. Each of these states, as required by matter parity, includes precisely two LIPs, as well as a number of jets, charged leptons, and neutrinos.

The presence of sizeable QCD backgrounds for final states involving one or more jets renders such states difficult to use for discovery; final states involving charged leptons alone, on the other hand, have far smaller SM backgrounds and hence are far more auspicious in terms of their LHC discovery potential. A single lepton plus missing E_T signal would be difficult to resolve, due to the huge SM W background, but a variety of multilepton signatures initiated by the electroweak processes enumerated above may be observable at the LHC. The trilepton + $\not{E}_T$ channel, for example, which is of crucial importance for supersymmetry searches [29], can potentially also be important in searching for an additional, inert scalar doublet. In this work, however, we will focus on the dilepton

TABLE II. Leading-order cross sections for the associated production of SA, H^+H^-, $SH^{\pm}$, and $AH^{\pm}$ at the LHC, with center-of-mass energy $\sqrt{s} = 14$ TeV, for the various benchmark points defined in Table I.

Benchmark	σ_{SA} (fb)	$\sigma_{H^+H^-}$ (fb)	$\sigma_{SH^{\pm}}$ (fb)	$\sigma_{AH^{\pm}}$ (fb)
LH1	289.2	69.8	503.3	125.2
LH2	628.8	163.6	1055.1	299.0
LH3	179.9	86.0	319.0	154.9
LH4	248.9	440.2	1050.3	370.1
LH5	465.5	93.3	352.9	302.3
HH1	91.8	2.9	25.4	13.5
HH2	152.0	4.0	33.0	20.5
HH3	336.7	5.6	43.7	35.2

channel, which seems to offer the brightest prospects for discovery.

The dominant signal contribution to $\ell^+\ell^- + \not{E}_T$ in the IDM, where $\ell = \{e, \mu\}$, results from either $pp \to SA$ with $A \to S\ell^+\ell^-$, or $pp \to H^+H^-$, with $H^\pm \to S\ell^\pm\nu$, depending on the choice of parameters. These processes are depicted diagrammatically in panels (a) and (b) of Fig. 1, respectively. Other processes that result in $\ell^+\ell^- + \not{E}_T$ final states, e.g. $pp \to H^+H^-$ with $H^+ \to S\ell^+\nu$ and $H^- \to A\ell^-\bar{\nu} \to S\ell^-\bar{\nu}\nu\bar{\nu}$, generally contribute only a small amount to the signal cross section and can therefore be safely ignored. Another contribution comes from processes in which a leptonically decaying pseudoscalar A is produced in association with some other particle or particles which decay to jets or charged leptons too soft to register in the detector. In general, the event rates for such processes (the most important of which is $pp \to H^\pm A \to \ell^+\ell^- jj + \not{E}_T$) are also small compared to that for $pp \to SA \to \ell^+\ell^- + \not{E}_T$. However, if δ_1 is small (as it is in benckmark LH4), a substantial fraction of the jets and charged leptons from $H^\pm$ decays will be sufficiently soft that such processes do yield a considerable contribution and therefore need to be accounted for in the analysis.

In addition to the pair-production processes discussed above, the electroweak Higgs-associated-production process

$$q\bar{q} \to hZ \tag{11}$$

can also result in a $\ell^+\ell^- + \not{E}_T$ final state in the manner illustrated in panel (c) of Fig. 1, as long as the decay $h \to SS$ is permitted. The dilepton-channel contribution from this process is significant only in cases in which λ_L is nonzero and $m_h > 2m_S$—the conditions under which h can decay on shell to a pair of LIPs. Of the eight benchmark scenarios defined in Table. I, these conditions are satisfied only in scenarios LH1 and LH2, for which $\sigma_{hZ} \times \mathrm{Br}(h \to SS) = 343.12$ fb and 706.65 fb, respectively. As these rates are roughly on the same order as those for $pp \to SA$ production, it will be necessary to take this contribution into account in the ensuing analysis.

A further contribution to the $\ell^+\ell^-\not{E}_T$ production cross section in the IDM results from $pp \to SSZ$ production via the four-point $SSZZ$ interaction shown in panel (d) of Fig. 1. However, this contribution is quite small in comparison with that from SA pair production, as the former is a three-body process while the latter is only two-body. Interference effects between the diagrams depicted in panels (a), (c), and (d) of Fig. 1 are consequently tiny as well, and can be safely neglected.

In what follows, we will focus on $pp \to SA \to \ell^+\ell^- SS$ as our signal process, and treat $pp \to H^+H^- \to \ell^+\ell^-\nu\bar{\nu}SS$ as part of the background. The reason for this is twofold. First, since the constraints in Sec. III (and especially those from WMAP and electroweak precision data) typically prefer situations in which $2m_{H^+} \gtrsim m_A + m_S$, production cross sections for $pp \to H^+H^-$ tend to be lower than those for $pp \to SA$. Second, a $pp \to H^+H^- \to \ell^+\ell^- + \not{E}_T$ signal turns out to be far more difficult to distinguish from the dominant SM backgrounds (discussed in detail below) on the basis of event topology. We will also treat $pp \to hZ \to SS\ell^+\ell^-$ and $pp \to SSZ \to SS\ell^+\ell^-$ as a contribution to the background, because the event topologies generally differ from those associated with $pp \to SA \to \ell^+\ell^- SS$.

The SM backgrounds relevant for the $\ell^+\ell^- + \not{E}_T$ channel are well known from studies of the supersymmetric

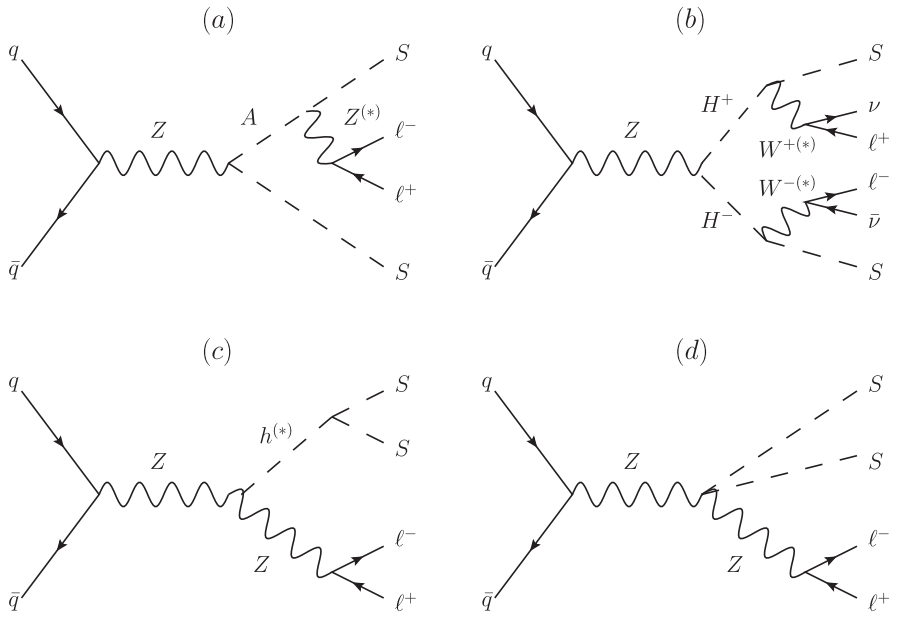

FIG. 1. Diagrams corresponding to the contributions to the $pp \to \ell^+\ell^-\not{E}_T$ in the IDM discussed in the text.

process $pp \to \chi_1^0 \chi_2^0 \to \ell^+\ell^- + \not{E}_T$, where χ_1^0 and χ_2^0 are the lightest and next-to-lightest neutralinos. These include irreducible backgrounds from WW and ZZ/γ^* production (with the contribution from off-shell photons [30] properly taken into account), as well as reducible backgrounds from $t\bar{t}$, WZ/γ^*, Wt, and $Zb\bar{b}$ processes; $WW + n$ jets and $ZZ + n$ jets; and Drell-Yan production of $\tau^+\tau^-$ pairs.

In the present analysis, events were generated at the parton level, both for the signal process and for the backgrounds discussed above, in MADGRAPH [31] and then passed through PYTHIA [32] for parton showering and hadronization. Events were then passed through PGS4 [33] to simulate the effects of a realistic detector. Subsequent to event generation, in order to distinguish signal events from those associated with these backgrounds and to account for the performance thresholds of the LHC detectors, we impose three sets of cuts in our analysis. The first such set, henceforth referred to as our Level I cuts, is designed to mimic a realistic detector acceptance:

(i) Exactly two electrons or muons with opposite charge.
(ii) $p_T^\ell \geq 15$ GeV and $|\eta_\ell| \leq 2.5$ for each of these charged leptons.
(iii) For lepton isolation, we require $\Delta R_{\ell\ell} \geq 0.4$ for the charged-lepton pair, and $\Delta R_{\ell j} \geq 0.4$ for each combination of one jet and one charged lepton.

It should be noted that for $\ell = \{e, \mu\}$, the above lepton p_T^ℓ cut is sufficient to meet the Level I triggering requirements for both ATLAS [34] and CMS [35].

The subsequent two sets of selection criteria we impose are designed to discriminate efficiently between signal and background events. Our Level II cuts are aimed at suppressing reducible backgrounds from processes such as $t\bar{t}$, WZ/γ^*, Wt, and $Zb\bar{b}$, which tend to involve either hard jets, little missing transverse energy, or both. We impose a veto on all events manifesting high-p_T jet activity within the central region of the detector, as well as a minimum missing transverse energy cut:

(i) No jets with $p_T^j > 20$ GeV and pseudorapidity within the range $|\eta_j| < 3.0$.
(ii) $\not{E}_T > 30$ GeV.

The efficacy of this latter missing E_T cut should not be overemphasized: while each signal event necessarily includes a pair of LIPs, these particles tend to be produced back-to-back. As a result, their contributions to the overall $\not{E}_T$ tend to cancel each other out, to the end that the $\not{E}_T$ distributions for signal events tend not to differ radically from those for processes like ZZ/γ^*, WW, and $t\bar{t}$ which involve energetic neutrinos. Nevertheless, this $\not{E}_T$ cut is highly efficient in eliminating background contributions from $Zb\bar{b}$ and WZ/γ^* events (with the W decaying hadronically) with jets soft enough so as to survive the central-jet veto.

After imposing Level I and II cuts, contributions from $Zb\bar{b}$ and Drell-Yan production of leptonically decaying $\tau^+\tau^-$ pairs, are effectively eliminated. The dominant remaining backgrounds are the irreducible ones from WW and ZZ/γ^* events, as well as residual $t\bar{t}$, WZ/γ^* and Wt events which survive the Level II cuts. In Table III, we list the signal cross sections for $pp \to SA \to \ell^+\ell^-\not{E}_T$ at the LHC for each of the benchmark points presented in Table I, after the application of the Level I and Level II cuts discussed in the previous section. We also show the effect that these cuts have on the cross sections for those background processes, both reducible and irreducible, which remain at non-negligible levels after the Level II cuts have been applied: WW, ZZ/γ^*, $t\bar{t}$, WZ/γ^*, and Wt. Results for $pp \to H^+H^- \to \ell^+\ell^-\not{E}_T$ and $pp \to h^{(*)}Z \to SS\ell^+\ell^-$, also treated as background processes in this analysis, are shown here as well. It is evident from the data presented in Table III that the application of the Level I + II cuts results in a substantial reduction of the reducible backgrounds from $t\bar{t}$, WZ/γ^*, and Wt. However, as efficient as these cuts are, the rates for these background processes (and especially from $t\bar{t}$) are large enough that a substantial number of events still survives them. Consequently, these reducible backgrounds cannot be neglected in the final analysis.

In order to differentiate the $pp \to SA$ signal from these remaining backgrounds, it is necessary to impose a third level of event-selection criteria based largely on event topology, whose thresholds can be adjusted to optimize significance of discovery in any given benchmark scenario. For the benchmark points included in our survey, the optimal pattern of Level III cuts generally falls into one of two categories, depending primarily on whether or not the decay of $A \to SZ^{(*)}$ occurs on shell.

In all of our benchmark scenarios in which $\delta_2 > M_Z$, the CP-odd scalar A decays essentially 100% of the time to an LIP and an on-shell Z; thus the distribution of the invariant mass $M_{\ell\ell}$ of the charged-lepton pair in such scenarios tends to peak sharply around M_Z. This is the case for points LH1 and HH1, the $M_{\ell\ell}$ distribution for the former of which is shown in the left panel of Fig. 2. It is therefore advantageous to select events on the basis of whether or not $M_{\ell\ell}$ falls within a window

(i) $M_{\ell\ell}^{\min} \leq M_{\ell\ell} \leq M_{\ell\ell}^{\max}$,

where the parameters $M_{\ell\ell}^{\min}$ and $M_{\ell\ell}^{\max}$ are to be adjusted to optimize the statistical significance of discovery for each benchmark point. In cases of this sort, the best results are generally obtained by imposing a window around 20 GeV wide, centered near M_Z. Such a cut efficiently reduces the W^+W^-, $Z\gamma^*$, $W\gamma^*$, $t\bar{t}$ and Wt backgrounds, leaving the ZZ and WZ backgrounds (which are little affected by such a cut) as the dominant ones.

In cases where $\delta_2 < M_Z$ (LH2–LH5, HH2–HH3), the two-body decay $A \to SZ$ is kinematically inaccessible. Likewise, the decay channel $A \to H^\pm W^\mp$ is not open unless $\delta_2 > \delta_1 + M_W$—a condition which is difficult to realize, given the constraints on the model, and which is not

TABLE III. Leading-order cross sections for the signal processes $pp \to SA \to \ell^+\ell^-\not{E}_T$ at the LHC with $\sqrt{s} = 14$ TeV after Level I and II cuts for each of the benchmark points presented in Table I. Also shown are the backgrounds $pp \to H^+H^- \to \ell^+\ell^-\not{E}_T$, $pp \to h^{(*)}Z \to \ell^+\ell^-\not{E}_T$, WW, ZZ/γ^*, $t\bar{t}$, WZ/γ^*, Wt after Level I + II cuts, as well as a total background cross section.

Benchmark	Level I Cuts			Level I + II Cuts			SM Backgrounds	Level I Cuts	Level I + II Cuts
	σ_{SA} (fb)	$\sigma_{H^+H^-}$ (fb)	σ_{hZ} (fb)	σ_{SA} (fb)	$\sigma_{H^+H^-}$ (fb)	σ_{hZ} (fb)		σ_{BG} (fb)	σ_{BG} (fb)
LH1	9.61	0.82	2.90	6.03	0.46	1.79	WW	621.44	316.97
LH2	10.28	1.06	5.75	6.53	0.51	3.47	ZZ/γ^*	132.09	76.46
LH3	2.32	0.34	0.01	1.47	0.13	0.01	$t\bar{t}$	4531.51	58.87
LH4	3.84	0.19	0	2.07	0.02	0	WZ/γ^*	113.97	51.85
LH5	0.38	~0	0.01	~0	0.14	0.01	Wt	709.14	52.11
HH1	3.23	0.02	0	1.97	0.01	0	Total SM Background	6108.15	556.26
HH2	3.01	0.03	0	1.81	0.01	0			
HH3	1.69	0.02	0	1.09	0.01	0			

satisfied for any of the benchmark points in our study. When these decays are unavailable, the dominant leptonic decay channel for the A involves the three-body process $A \to S\ell^+\ell^-$, which proceeds through an off-shell Z. As a result, the dilepton invariant mass distribution is peaked well below M_Z, around the value of δ_2, as shown in the right panel of Fig. 2 for benchmark point LH3. In cases of this sort, imposing an upper limit $M_{\ell\ell}^{\max} \sim \delta_2$ on the dilepton invariant mass can assist in improving the signal-to-background ratio. A cut of this sort can effectively suppress the ZZ and WZ backgrounds, the $M_{\ell\ell}$ distributions for which are peaked sharply around M_Z.

To further suppress the standard-model WW, $Z\gamma^*$, $W\gamma^*$, Wt, and $t\bar{t}$ backgrounds in cases in which $\delta_2 < M_Z$, it is useful to select events on the basis of observables related to the angular separation between charged leptons. The ℓ^+ and ℓ^- produced by these SM background processes are typically energetic and well-separated from one another. On the other hand, those resulting from A decay via an off-shell Z tend to be soft, with small (and extremely so, if δ_2 is quite small) angular separation. This difference in event topology is readily apparent from Fig. 3, which displays the $\Delta R_{\ell\ell}$ (left panel) and $\cos\phi_{\ell\ell} \equiv \cos(\phi_{\ell^+} - \phi_{\ell^-})$ (right panel) distributions for benchmark LH3. It is therefore useful, in cases in which $\delta_2 < M_Z$, to impose the additional cuts

(i) $\Delta R_{\ell\ell} \leq \Delta R_{\ell\ell}^{\max}$,
(ii) $\cos\phi_{\ell\ell} \geq \cos\phi_{\ell\ell}^{\min}$,

where $\Delta R^{\max}$ and $\cos\phi_{\ell\ell}^{\min}$ are to be optimized for each benchmark point.

In certain situations, the imposition of additional event-selection criteria can also be helpful in distinguishing signal from background events. For example, it can also be advantageous to impose a minimum cut on the total transverse momentum variable

$$H_T \equiv \not{p}_T + \sum_i p_T^{\ell_i}, \tag{12}$$

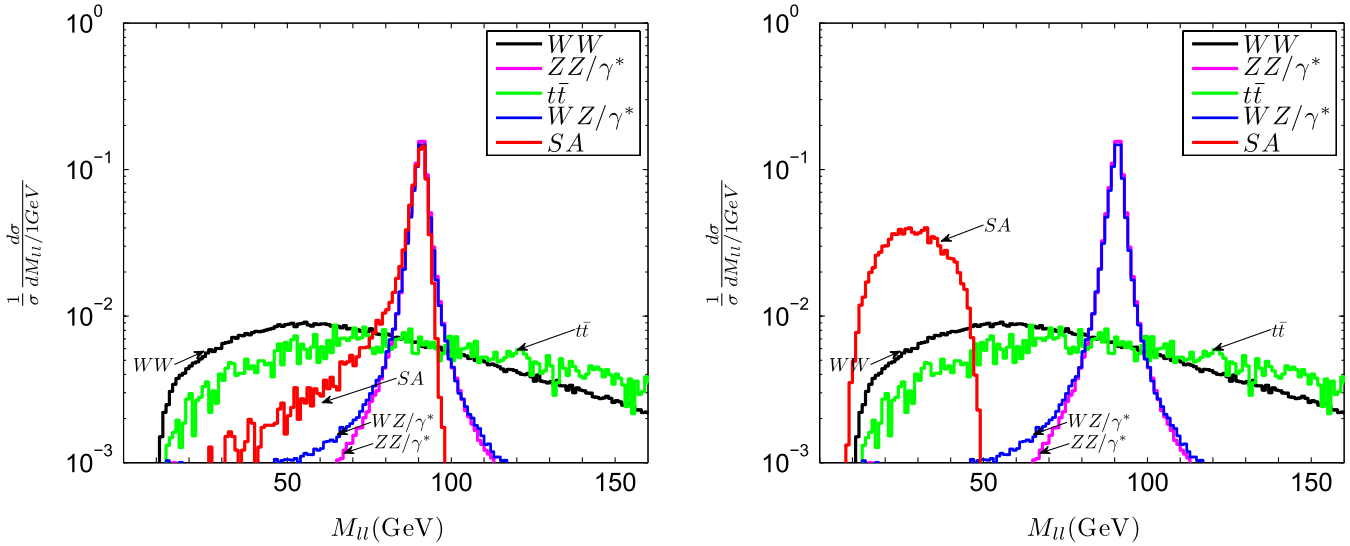

FIG. 2 (color online). Dilepton-invariant-mass distributions for the benchmark points LH1 (left panel) and LH3 (right panel) both for the signal process and for the most relevant SM backgrounds.

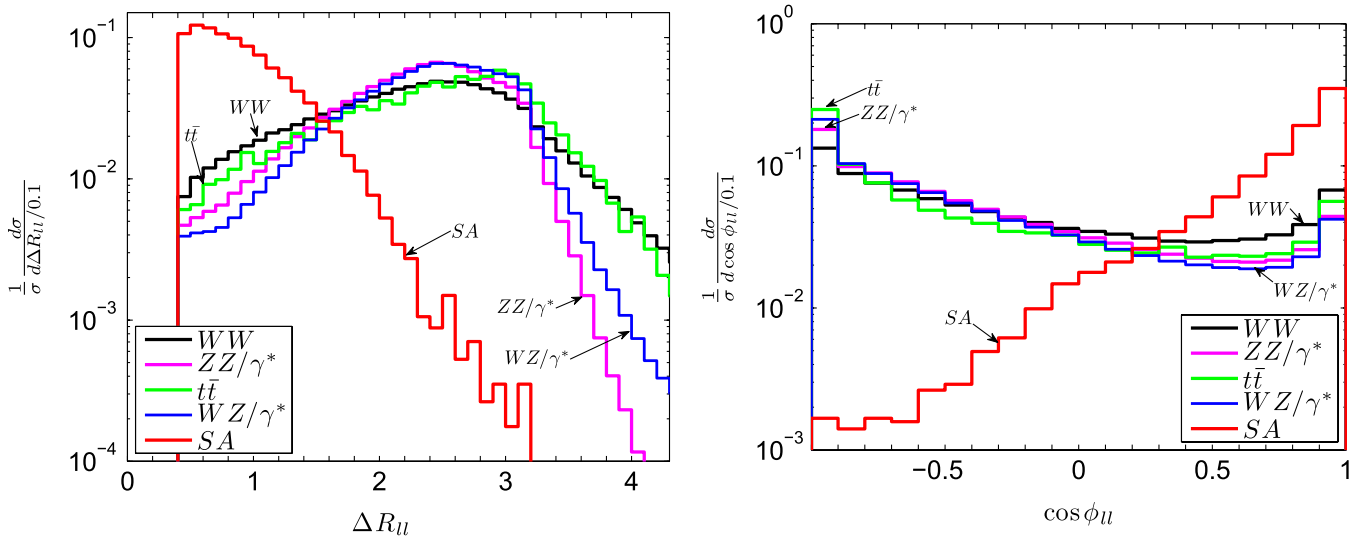

FIG. 3 (color online). Distributions of the angular-separation variables $\Delta R_{\ell\ell}$ (left panel) and $\cos\phi_{\ell\ell}$ (right panel) for benchmark point LH3, in which decays of the pseudoscalar A occur via an off-shell Z. These distributions justify the imposition of the minimum $\cos\phi_{\ell\ell}$ and maximum $\Delta R_{\ell\ell}$ cuts described in the text.

TABLE IV. A list of the optimized Level III cuts used in the analysis of each of the benchmark points presented in Table I. An entry of "-" indicates that the corresponding cut is not imposed. Note that a $\not{E}_T^{\rm min}$ cut of 30 GeV has been applied in each of these scenarios as a part of the Level II cuts, but that this threshold has been raised for several of the points at Level III. For more details on the definition of the thresholds used, see text.

Benchmark	$M_{\ell\ell}^{\rm min}$	$M_{\ell\ell}^{\rm max}$	$\Delta R_{\ell\ell}^{\rm max}$	$\cos\phi_{\ell\ell}^{\rm min}$	$H_T^{\rm min}$	$\not{E}_T^{\rm min}$	$p_{T\ell}^{\rm max}$
LH1	80 GeV	100 GeV	-	-	150 GeV	50 GeV	-
LH2	-	70 GeV	1.2	0.7	200 GeV	100 GeV	-
LH3	20 GeV	50 GeV	0.8	0.7	200 GeV	90 GeV	-
LH4	20 GeV	50 GeV	0.8	0.7	200 GeV	90 GeV	-
LH5	-	10 GeV	0.6	0.9	-	30 GeV	25 GeV
HH1	80 GeV	100 GeV	2.0	-	200 GeV	80 GeV	-
HH2	20 GeV	70 GeV	1.2	0.7	200 GeV	90 GeV	
HH3	-	25 GeV	-	-	-	30 GeV	-

TABLE V. Cross sections for the processes $pp \to SA \to \ell^+\ell^-\not{E}_T$, $pp \to H^+H^- \to \ell^+\ell^-\not{E}_T$, and $pp \to h^{(*)}Z \to \ell^+\ell^-\not{E}_T$ at the LHC for each of the benchmark points presented in Table I after the application of our Level III cuts. Cross sections for the dominant SM backgrounds (WW, ZZ/γ^*, etc.) after the application of the Level III cuts are also shown, as is the total background cross section including all of these individual contributions. An entry of "$\sim$0" indicates a cross section less than 1 ab. The last two columns display the signal-to-background ratio S/B and statistical significance (as given by $S/\sqrt{B}$) corresponding to an integrated luminosity of $\mathcal{L} = 100$ fb^{-1} after the application of these same cuts.

Benchmark	Level III Cuts									S/B	$S/\sqrt{B}$
	σ_{SA} (fb)	$\sigma_{H^+H^-}$ (fb)	σ_{hZ} (fb)	σ_{WW} (fb)	σ_{ZZ/γ^*} (fb)	$\sigma_{t\bar{t}}$ (fb)	σ_{WZ/γ^*} (fb)	σ_{Wt} (fb)	$\sigma_{\rm BG}^{\rm comb}$ (fb)		
LH1	3.42	0.04	1.28	11.59	36.99	4.55	19.52	3.82	77.79	0.04	3.87
LH2	0.89	$\sim$0	0.01	0.07	0.24	0.11	0.08	0.07	0.58	1.53	11.66
LH3	0.18	$\sim$0	$\sim$0	0.03	0.15	0.05	0.04	0.06	0.34	0.52	3.04
LH4	0.19	$\sim$0	0	0.03	0.15	0.05	0.04	0.06	0.34	0.57	3.29
LH5	0.004	$\sim$0	$\sim$0	0.13	0.04	$\sim$0	0.04	0.01	0.23	0.02	0.02
HH1	0.65	$\sim$0	0	0.45	13.41	0.55	5.85	0.45	20.71	0.03	1.42
HH2	0.37	0.01	0	0.08	0.26	0.12	0.09	0.12	0.67	0.56	4.55
HH3	1.01	$\sim$0	0	17.49	1.06	1.60	0.76	1.65	22.56	0.04	2.12

which can serve as an efficient discriminant in both the $\delta_2 > M_Z$ and $\delta_2 < M_Z$ cases:

(i) $H_T \geq H_T^{\min}$.
Again, the threshold $H_T^{\min}$ can be optimized to suit a given benchmark point. This cut can be helpful in reducing the WW and $Z\gamma^*$ backgrounds, but is less so in reducing the contribution from $t\bar{t}$. In addition, it can sometimes also be useful to tighten the minimum $\not{E}_T$ cut applied during the Level II cuts. Therefore, at Level III, we allow for the imposition of an additional missing-transverse-energy cut.

(ii) $\not{E}_T \geq \not{E}_T^{\min}$.
Furthermore, in cases in which δ_2 is small and the charged leptons associated with the signal process far less energetic than those associated with the SM backgrounds, it can be useful to impose a ceiling $p_{T\ell}^{\max}$ on the p_T of each charged lepton, as we do here for benchmark point LH5.

(iii) $p_{T\ell} \leq p_{T\ell}^{\max}$.
In Table IV, we list the Level III cuts applied in each of the benchmark scenarios listed in Table I. The precise numbers appearing in this table have been selected in order to maximize the $S/\sqrt{B}$ ratio for each individual benchmark point. It should be noted that the particular set of cuts applied in each case indeed depends primarily on the relationship between δ_2 and M_Z.

V. RESULTS

Now that we have discussed in detail the event-selection procedure to be used in our numerical analysis of dilepton signals in the IDM, we turn to present the results of that numerical analysis. In Table V, we list the cross sections[4] for the signal process and the most relevant backgrounds after the application of our Level I + II + III cuts. The last two columns in the Table display the signal-to-background ratio S/B and the statistical significance (as given by $S/\sqrt{B}$ at an integrated luminosity of $\mathcal{L} = 100$ fb^{-1}) for each benchmark point[5] in our analysis, after the implementation of these same cuts. Note that the numbers quoted here for benchmark LH4 with small δ_1 include, in addition to the usual $pp \to SA \to \ell^+\ell^- + \not{E}_T$ contribution, contributions from the processes $pp \to H^\pm A \to \ell^+\ell^- jj + \not{E}_T$ and $pp \to H^\pm A \to \ell^+\ell^-\ell^\pm + \not{E}_T$ in which the additional jets or leptons from $H^\pm$ decay are sufficiently soft as to escape detection. It should be noted that taking these contributions into account results in an increase in the statistical significance of discovery in this channel from 2.07σ to 3.29σ. For the other benchmark points listed in Table I, $\delta_1 \geq 50$ GeV, and consequently the contribution from $pp \to H^\pm A$ processes with soft jets or leptons will be negligible.

Let us now turn to examine the results for each of the individual benchmark scenarios in our study in more detail. We begin with the point LH1, which involves a light Higgs boson, a light LIP ($m_S \sim 40$ GeV), and a large mass splitting ($\delta_2 = 100$ GeV $> M_Z$). The dominant backgrounds in this scenario are those from ZZ and WZ, each of which also involves the leptonic decay of an on-shell Z and is therefore difficult to differentiate from the signal process on the basis of kinematical variables. The remaining backgrounds are efficiently suppressed after the imposition of the $M_{\ell\ell}$ cut near the M_Z window. With 100 fb^{-1} of integrated luminosity, a significance level of 3.87σ could be obtained in this benchmark scenario. The situation for the heavy-Higgs benchmark HH1 is similar; however the smaller SA-production cross section in this case (due primarily to an increased LIP mass) translates into a lower statistical significance.

Benchmark point LH2 also includes a 40 GeV dark-matter particle, but involves a smaller mass splitting than that of LH1: $\delta_2 = 70$ GeV. This scenario affords the best opportunity for discovery at the LHC out of any of the benchmark points in our analysis, yielding a statistical significance of 11.66σ with 100 fb^{-1} of integrated luminosity. Two factors contribute to its success: a small production threshold $m_S + m_A$, and the fact that $\delta_2 < M_Z$, which implies that the CP-odd scalar A decays via an off-shell Z. The latter consideration makes it possible to eliminate ZZ and WZ background contributions quite efficiently by setting $M_{\ell\ell}^{\max}$ comfortably below the Z pole. Further cuts on the angular variables $\cos\phi_{\ell\ell}$ and $\Delta R_{\ell\ell}$ serve to reduce the remaining backgrounds to a manageable level. After all cuts are imposed, events from the low-$M_{\ell\ell}$ tail of the ZZ distribution form the dominant background. It should be noted, however, that while the aforementioned angular-separation cuts are quite efficient in reducing background events, this efficiency comes with a price: the cuts also eliminate a substantial fraction of signal events. This explains why the signal cross section for LH2 is less than that for LH1, as no angular-separation cuts are imposed in the latter scenario.

Benchmarks LH3 and LH4 are superficially similar, given that they involve a similar LIP mass $m_S \sim 80$ GeV and the same mass splitting $\delta_2 = 50$ GeV. In this case,

[4]The cross sections given here are evaluated at leading order (LO). Next-to-leading-order (NLO) results for the relevant backgrounds are provided in [36]. An estimate of the signal K-factor at NLO can be obtained by from the analysis performed in Ref. [37] for Drell-Yan H^0A production in the context of two-Higgs-doublet models, which is analogous to the SA production process considered here. Taking both signal and background K-factors into account, one finds $S/\sqrt{BG}$ for any given process at NLO to be roughly 85–100% of the LO result; hence, the results at NLO will not differ substantially from the LO results presented here.

[5]One modification is made in the case of LH5. For this point, both signal and background event rates are quite low, and consequently the significance value quoted in the last column of Table V was obtained using Poisson statistics rather than $S/\sqrt{B}$.

however, the marked difference in δ_1—a parameter which generally has little effect on observability of the dilepton signal in the *SA* associated-production channel—between the two points has a substantial impact on their collider phenomenology. The reason for this is twofold. First of all, since $\delta_2 > \delta_1$ for LH4 (unlike any other benchmark in our analysis), the decay channels $A \to H^{\pm} W^{\mp} \to X + \not{E}_T$, where X denotes either four jets, two jets and a single charged lepton, or two charged leptons, are open in this scenario, with a branching ratio $\mathrm{BR}(A \to H^{\pm} W^{\mp} \to X + \not{E}_T) = 0.435$. As a result, $\mathrm{BR}(A \to SZ \to \ell^+ \ell^- + \not{E}_T)$, and thus the dilepton-signal cross section, are reduced by an additional factor of 2 relative to those points for which such competing decays are kinematically prohibited. Second of all, as discussed above, the small value for $\delta_1 = 10$ GeV in LH4 allows the additional contribution of $AH^{\pm}$ process to the signal due to the unobservable soft jets and leptons from $H^{\pm}$ decay. These additional contributions augment the overall signal cross section and more than compensate for the diminished $\mathrm{BR}(A \to SZ \to \ell^+ \ell^- + \not{E}_T)$, as discussed above. For 100 fb^{-1} of integrated luminosity, a significance level greater than 3σ could be reached for LH4 as well as LH3.

The final light-Higgs scenario in our analysis, LH5, turns out to be the most difficult benchmark point for which to observe a dilepton signal, primarily because of the small mass splitting $\delta_2 = 10$ GeV between S and A. The charged leptons in the final state tend to be extremely soft, and consequently the signal remains buried under the SM background even after an optimized set of Level III cuts is applied. Scenarios with a small value of δ_2 will in general be difficult to discover via this channel at the LHC. It should be noted that the results we obtain for this benchmark differ significantly from the parton-level results quoted in [18] for a similar benchmark scenario, also with $\delta_2 = 10$ GeV. The discrepancy owes primarily to our imposition of a Level I cut of $\Delta R_{\ell\ell} > 0.4$ cut designed to replicate the effect of electron and muon isolation requirements at the ATLAS and CMS detectors. Since the angular separation between the lepton momenta tends to be extremely small for such a small value of δ_2, a vast majority of signal events will have $\Delta R_{\ell\ell} < 0.4$ and hence be eliminated by this cut.

Let us now turn to discuss the benchmark points which feature a heavy ($m_h = 500$ GeV) Higgs boson—in other words, those benchmarks for which the IDM successfully addresses the LEP paradox. While the electroweak precision constraints discussed in Sec. III are more stringent in this case, these constraints primarily affect δ_1, which is typically required to be quite large. Since this parameter generally does not affect results in the dilepton channel, which depend primarily on m_S and δ_2, the same qualitative results obtained for the light-Higgs benchmarks also apply here. For HH1, with $\delta_2 = 100$ GeV, a significance level of only 1.42σ can be achieved with 100 fb^{-1} of integrated luminosity, due to both the overwhelming SM backgrounds that exist for dilepton processes involving on-shell Z decay, and a suppressed signal cross section relative to benchmark LH1 (which has a far lighter LIP). For HH3—a benchmark with a somewhat small value of δ_2—a $M_{\ell\ell}^{\max} = 25$ GeV cut helps to cut down the SM backgrounds from processes involving on-shell Z decay. It is, however, hard to improve upon the statistical significance by implementing additional cuts. The remaining background events which survive this cut (most of which come from WW) tend to have similar $\cos\phi_{\ell\ell}$ and $\Delta R_{\ell\ell}$ distributions to those of the signal—a situation which makes the application of further, angular cuts essentially redundant. Furthermore, since the missing-energy distribution for the signal events in scenarios with small δ_2 peaks at relatively low values of $\not{E}_T$, there is little to be gained by increasing $\not{E}_T^{\min}$ much beyond the Level II threshold of 30 GeV. By contrast, in scenarios with larger δ_2, an elevated missing-energy cut works quite effectively in tandem with the angular cuts in reducing backgrounds from WW and $t\bar{t}$. A significance level of 2.32σ is reached for HH3 with 100 fb^{-1} of integrated luminosity.

It is benchmark HH2, however, which affords the best opportunity for discovery at the LHC from among the heavy-Higgs scenarios, with a statistical significance of 4.55σ at 100 fb^{-1} of integrated luminosity. This is because the signal for this benchmark can be distinguished from the WZ and ZZ backgrounds on the basis of $M_{\ell\ell}$ cuts, and from the remaining WW, Wt, and $t\bar{t}$ backgrounds on the basis of $\cos\phi_{\ell\ell}$, $\Delta R_{\ell\ell}$, and $\not{E}_T$ cuts in the same manner as for the low-Higgs-mass point LH2. We therefore conclude that even scenarios in which the IDM permits an evasion of the LEP upper bound on m_h can yield an observable dilepton signal at the LHC.

From the results in Table V, it is evident that the prospects for detecting a signal in the dilepton channel in the IDM model hinge primarily on two criteria. The first of these is the dependence of the cross section for $q\bar{q} \to SA$ on $m_S + m_A$ and δ_2. This cross section is, of course, larger in cases where the pair-production threshold energy $m_S + m_A$ is small. Among cases with similar values of $m_S + m_A$, those in which δ_2 is smaller will have larger production cross sections. This can be understood by noting that the partonic cross section for this process depends on m_S and δ_2 in the following way:

$$\hat{\sigma}_{q\bar{q}\to SA}(\hat{s}) \propto [\hat{s}^2 - 2\hat{s}(\delta_2(\delta_2 + 2m_S) + 2m_S^2) + \delta_2^2(\delta_2 + 2m_S)^2]^{3/2}. \tag{13}$$

For values of $\sqrt{\hat{s}} \sim m_S + m_A$, for which the dependence of this expression on m_S and δ_2 is non-negligible, it is apparent that for fixed $m_S + m_A$, $\hat{\sigma}_{q\bar{q}\to SA}(\hat{s})$ decreases with increasing δ_2. This accounts for the difference between the $pp \to SA$ production cross sections for benchmarks LH1 and HH3 quoted in Table II.

The second criterion is the relationship between δ_2 and M_Z: cases in which $\delta_2 < M_Z$ tend to have a higher statistical significance than those in which $\delta_2 > M_Z$, as is manifest from comparing the results for benchmarks LH2 and LH1 in Table V. This is because in the latter case, it is difficult to distinguish the signal process from the dominant ZZ background on the basis of event topology. On the other hand, when δ_2 is exceedingly small (as it is in our LH5 scenario), the charged leptons will be so soft that the detector-acceptance (i.e. Level I) cuts will eliminate the vast majority of would-be signal events, as discussed above. Between these extremes, a window of

$$40\ \text{GeV} \lesssim \delta_2 \lesssim 80\ \text{GeV} \tag{14}$$

emerges within which the prospects for observing a signal are quite good, so long as the LIP mass also falls roughly within the 40–80 GeV range. For cases in which $\delta_2 \gtrsim M_Z$, the prospects for discovery at the LHC are reasonable—meaning a statistical significance around the 3σ level with 100 fb^{-1} of integrated luminosity—only if the dark-matter particle is light ($m_S \sim 40$ GeV).

It is not difficult simultaneously to satisfy the constraints discussed in Sec. III and to realize a δ_2 value within this mass window of 40–80 GeV while keeping the LIP mass relatively light ($m_S \lesssim 80$ GeV)—or, alternatively, to obtain a large mass splitting $\delta_2 \gtrsim M_Z$ and a light LIP mass of around 40 GeV. This is true not only in models where the Higgs boson is light and the parameters of the theory comparatively unconstrained, but also in cases in which the mechanism of Ref. [2] for evading electroweak precision bounds on the Higgs mass is realized in nature, and $m_h \sim 500$ GeV. In either case, it would be possible to observe a dilepton signal at the LHC at a significance level of 3σ or higher, with an integrated luminosity of 100 fb^{-1}.

In light of recent developments concerning the maximum center-of-mass energy the LHC will likely achieve, it is worth commenting briefly on how the detection prospects would be impacted by lowering $\sqrt{s}$ from 14 TeV to 7 TeV or 10 TeV. At $\sqrt{s} = 7$ GeV, production cross sections would be substantially lowered, and a large increase in integrated luminosity (greater than that which would ever be accumulated at the LHC) would likely be required to obtain an observable signal in all but the most auspicious cases. At $\sqrt{s} = 10$ TeV, the cross sections for both the signal process and the most relevant SM backgrounds are roughly 50–60% of what they are at 14 TeV. Consequently, one can estimate that $S/\sqrt{BG}$ for a given benchmark will be roughly 70% of the corresponding statistical significance value at 14 TeV, given the same integrated luminosity. The prospects for observing evidence of an inert doublet at $\sqrt{s} = 10$ TeV are therefore still reasonably auspicious.

VI. CONCLUSION

In this work, we have investigated the potential for observing a dilepton signature in the inert doublet model at the LHC. We have explored the prospects for a number of benchmark scenarios, including several in which the IDM successfully ameliorates the LEP paradox and the Higgs-boson mass can be elevated as high as $m_h = 400$–500 GeV, as well as several of the dark-matter motivated scenarios cataloged in Ref. [9]. We have shown that for cases in which the dark-matter candidate is relatively light (40–80 GeV) and 40 GeV $\lesssim \delta_2 \lesssim 80$ GeV, a signal with a significance of more than 3σ should be apparent at the LHC with less than 100 fb^{-1} of integrated luminosity. Moreover, in cases when the LIP is on the lighter end of this range, a 3σ discovery would be possible with only 10 fb^{-1} of integrated luminosity. In addition, there are also certain cases in which $\delta_2 > M_Z$ and the LIP is light ($m_S \sim 40$ GeV) for which the prospects for detection are also reasonably good.

Of course the observation of an excess in the $\ell^+\ell^- + \not{E}_T$ channel alone, while exciting, is by no means conclusive evidence for the inert doublet model. Indeed, many models of beyond-the-standard-model physics lead to such a signature, including weak-scale supersymmetry, two-Higgs-doublet models, etc. Fortunately, evidence for the IDM can come from a number of other sources. Some of these sources involve other channels associated with the SM-like Higgs at the LHC. One potentially interesting signal could arise due to deviations of the decay properties of the Higgs boson h from those of a SM Higgs. In situations in which $m_h > 2m_S$, for example, $\Gamma(h \to SS)$ can contribute substantially to the invisible Higgs width. Searches for the Weak-Boson Fusion (WBF) process $qq' \to qq'h$, with h decaying invisibly, can be used effectively to identify a Higgs boson at the LHC [38], and preliminary studies [18] indicate that a 5σ discovery should be possible with only 10 fb^{-1} of integrated luminosity in regions of parameter space where BR($h \to$ invisible) is large. Moreover, if $m_h > 2m_A$, the tetralepton + $\not{E}_T$ signatures resulting from decays of the form $h \to AA \to SS\ell^+\ell^-\ell^+\ell^-$ may also be detectable in certain regions of parameter space. The observation of signals of this sort, along with the nonobservation of other signals which appear in standard 2HDM due to $\phi_i \bar{f} f'$ couplings (where $\phi_i = H^\pm$, A, S and f and f' are SM fermions) absent in the inert doublet model, could together serve to distinguish the IDM from other scenarios for physics beyond the standard model.

Evidence for the IDM could also come from a variety of other sources, including dark-matter-direct-detection experiments and from the observation of energetic gamma rays [13,14] or neutrinos [10] resulting from LIP dark-matter annihilation. Clearly, the particular set of signals that an inert doublet would manifest differs substantially, depending on which of the allowed regions of parameter space the model happened to inhabit, and as we have shown, the $\ell^+\ell^- + \not{E}_T$ channel can provide an important probe into which region that might be.

ACKNOWLEDGMENTS

We would like to thank J. Alwall and T. Han for useful discussions and comments. We would like to thank the Aspen Center of Physics, where part of this work was completed. This work was supported in part by the Department of Energy under Grant No. DE-FG02-04ER-41298.

[1] N. G. Deshpande and E. Ma, Phys. Rev. D **18**, 2574 (1978).
[2] R. Barbieri, L. J. Hall, and V. S. Rychkov, Phys. Rev. D **74**, 015007 (2006).
[3] M. E. Peskin and T. Takeuchi, Phys. Rev. D **46**, 381 (1992).
[4] M. W. Grunewald, J. Phys. Conf. Ser. **110**, 042008 (2008).
[5] E. Ma, Phys. Rev. D **73**, 077301 (2006).
[6] T. Hambye and M. H. G. Tytgat, Phys. Lett. B **659**, 651 (2008).
[7] M. Lisanti and J. G. Wacker, arXiv:0704.2816.
[8] L. Lopez Honorez, E. Nezri, J. F. Oliver, and M. H. G. Tytgat, J. Cosmol. Astropart. Phys. 02 (2007) 028.
[9] E. M. Dolle and S. Su, Phys. Rev. D **80**, 055012 (2009).
[10] P. Agrawal, E. M. Dolle, and C. A. Krenke, Phys. Rev. D **79**, 015015 (2009).
[11] S. Andreas, M. H. G. Tytgat, and Q. Swillens, J. Cosmol. Astropart. Phys. 04 (2009) 004.
[12] E. Nezri, M. H. G. Tytgat, and G. Vertongen, J. Cosmol. Astropart. Phys. 04 (2009) 014.
[13] M. Gustafsson, E. Lundstrom, L. Bergstrom, and J. Edsjo, Phys. Rev. Lett. **99**, 041301 (2007).
[14] E. Dolle and S. Su (unpublished).
[15] D. Majumdar and A. Ghosal, Mod. Phys. Lett. A **23**, 2011 (2008).
[16] S. Andreas, T. Hambye, and M. H. G. Tytgat, J. Cosmol. Astropart. Phys. 10 (2008) 034; C. Arina, F. S. Ling, and M. H. G. Tytgat, J. Cosmol. Astropart. Phys. 10 (2009) 018.
[17] D. Aristizabal Sierra, J. Kubo, D. Restrepo, D. Suematsu, and O. Zapata, Phys. Rev. D **79**, 013011 (2009).
[18] Q. H. Cao, E. Ma, and G. Rajasekaran, Phys. Rev. D **76**, 095011 (2007).
[19] W. M. Yao *et al.*, J. Phys. G **33**, 1 (2006), partial update for 2008 available at http://pdg.lbl.gov/.
[20] (LEP Higgs Working for Higgs Boson Searches, ALEPH Collaboration, DELPHI Collaboration, CERN-L3 Collaboration, and OPAL Collaboration), arXiv:hep-ex/0107032.
[21] (LEP Higgs Working Group for Higgs Boson Searches, ALEPH Collaboration, DELPHI Collaboration, L3 Collaboration, and OPAL Collaboration, arXiv:hep-ex/0107031; J. Abdallah *et al.* (DELPHI Collaboration), Eur. Phys. J. C **34**, 399 (2004).
[22] A. Abulencia *et al.* (CDF Collaboration), Phys. Rev. Lett. **96**, 042003 (2006).
[23] M. Acciarri *et al.* (L3 Collaboration), Phys. Lett. B **472**, 420 (2000); R. Barate *et al.* (ALEPH Collaboration), Phys. Lett. B **499**, 67 (2001); J. Abdallah *et al.* (DELPHI Collaboration), Eur. Phys. J. C **31**, 421 (2003); G. Abbiendi *et al.* (OPAL Collaboration), Eur. Phys. J. C **35**, 1 (2004).
[24] LEP SUSY Working Group, http://lepsusy.web.cern.ch/lepsusy, LEPSUSYWG/01-03.1.
[25] E. Lundstrom, M. Gustafsson, and J. Edsjo, Phys. Rev. D **79**, 035013 (2009).
[26] A. Pierce and J. Thaler, J. High Energy Phys. 08 (2007) 026.
[27] ALEPH Collaboration , DELPHI Collaboration, L3 Collaboration, OPAL Collaboration, SLD Collaboration, LEP Electroweak Working Group, SLD Electroweak Group, and SLD Heavy Flavour Group,Phys. Rep. **427**, 257 (2006).
[28] D. N. Spergel *et al.* (WMAP Collaboration), Astrophys. J. Suppl. Ser. **148**, 175 (2003).
[29] R. Arnowitt and P. Nath, Mod. Phys. Lett. A **2**, 331 (1987); H. Baer and X. Tata, Phys. Rev. D **47**, 2739 (1993); H. Baer, C. Kao, and X. Tata, Phys. Rev. D **48**, 5175 (1993); T. Kamon, J. Lopez, P. McIntyre, and J. T. White, Phys. Rev. D **50**, 5676 (1994); H. Baer, C.-h. Chen, C. Kao, and X. Tata, Phys. Rev. D **52**, 1565 (1995); S. Mrenna, G. L. Kane, G. D. Kribs, and J. D. Wells, Phys. Rev. D **53**, 1168 (1996); K. T. Matchev and D. M. Pierce, Phys. Lett. B **467**, 225 (1999); Phys. Rev. D **60**, 075004 (1999).
[30] K. T. Matchev and D. M. Pierce, Phys. Lett. B **467**, 225 (1999).
[31] J. Alwall *et al.*, J. High Energy Phys. 09 (2007) 028.
[32] T. Sjostrand, S. Mrenna, and P. Skands, J. High Energy Phys. 05 (2006) 026.
[33] "PGS-Pretty Good Simulator," http://www.physics.ucdavis.edu/~conway/research/software/pgs/pgs4-general.html.
[34] (ATLAS Collaboration), Report No. ATLAS-TDR-14; (ATLAS Collaboration), Report No. ATLAS-TDR-15.
[35] G. L. Bayatian *et al.* (CMS Collaboration), J. Phys. G **34**, 995 (2007).
[36] Yu. M. Andreev, S. I. Bityukov, N. V. Krasnikov, and A. N. Toropin, Phys. At. Nucl. **70**, 1717 (2007).
[37] S. Dawson, S. Dittmaier, and M. Spira, Phys. Rev. D **58**, 115012 (1998).
[38] O. J. P. Eboli and D. Zeppenfeld, Phys. Lett. B **495**, 147 (2000).